

Resonant inelastic scattering spectra at the Ir L -edge in Na_2IrO_3

Jun-ichi Igarashi¹ and Tatsuya Nagao²

¹*Faculty of Science, Ibaraki University, Mito, Ibaraki 310-8512, Japan*

²*Faculty of Engineering, Gunma University, Kiryu, Gunma 376-8515, Japan*

(Dated: June 28, 2016)

We analyze resonant x-ray scattering (RIXS) spectra in Na_2IrO_3 on the basis of the itinerant electron picture. Employing a multi-orbital tight-binding model on a honeycomb lattice, we find that the zigzag magnetic order is the most stable with sizable energy gap in the one-electron band within the Hartree-Fock approximation. We derive the RIXS spectra, which are connected to the generalized density-density correlation function. We calculate the spectra as a function of excitation energy ω , within the random phase approximation. The spectra consist of the peaks with $\omega < 20$ meV, and of the peaks with $0.4 < \omega < 0.8$ eV. The former peaks are composed of four bound states in the density-density correlation function, and may be identified as the magnetic excitations, while the latter peaks are composed of sixteen bound states below the energy continuum of individual electron-hole pair excitations, and may be identified as the excitonic excitations. The calculated spectra agree qualitatively with the recent RIXS experiment.

PACS numbers: 71.10.Fd 75.30.Gw 71.10.Li 71.20.Be

I. INTRODUCTION

Resonant inelastic x-ray scattering (RIXS) has attracted much interest as a useful tool probing the elementary excitations in the materials¹⁻⁴. It could directly access to the d states in transition-metal compounds by using the L -edge resonance. The magnetic excitations have been clearly detected due to recent instrumental improvement of the energy resolution⁵⁻⁷. In this respect, RIXS could be compared with inelastic neutron scattering (INS). In particular, RIXS provides a valuable tool for the study of magnetic order when some isotopes show strong neutron absorption. Iridium, for instance, is the case where its main isotopes are strong neutron absorbers.

Recently, the elementary excitations in iridium oxides, such as CaIrO_3 ⁸, Sr_2IrO_4 ⁹, and Na_2IrO_3 ^{10,11}, have been investigated by RIXS experiments. Such $5d$ transition-metal compounds have drawn much attention, since their physical properties would be quite different from those of the $3d$ transition-metal compounds because of the competition between the large spin-orbit interaction (SOI) and the Coulomb interaction. Among them, we focus on Na_2IrO_3 in this paper. Its crystal structure belongs to the space group $C2/m$ ¹²⁻¹⁴, where Ir^{4+} ions constitute approximately two-dimensional honeycomb lattice with a Na ion located at its center. It is revealed to be a magnetic insulator with a zigzag spin order on the honeycomb lattice^{12,13,15-17}. In the RIXS experiment, the spectra as a function of excitation energy ω show peaks with $\omega < 35$ meV^{10,11}, which may be associated with the magnetic excitations. The INS experiment has detected similar peaks much lower region below 6 meV¹². In addition, there exist peaks with $0.4 < \omega < 0.8$ eV^{10,11}, which may be associated with the excitonic excitations.

The spin order as well as the magnetic excitations have been studied theoretically on the basis of the localized electron picture. In these studies, spin models of Kitaev-

Heisenberg type with the spin-orbital coupled isospin $j_{\text{eff}} = \frac{1}{2}$ ¹⁸⁻²² and of more generic types of models²³⁻²⁵ have been introduced. On the other hand, the band structure calculations based on the density functional theory (DFT) have been carried out²⁶⁻²⁸. By making the self-interaction correction (SIC) to the DFT, it is found that the zigzag spin order is realized as the ground state, and that the energy band has an energy gap ~ 0.5 eV²⁸. Although such itinerant-electron approaches look promising, the elementary excitations have not been calculated yet along this line. In our previous paper, employing a tight-binding model on a honeycomb lattice, we have calculated the generalized density-density correlation function within the random phase approximation (RPA) on a zigzag spin ordered ground state given by the Hartree-Fock approximation (HFA)²⁹. Though the calculated correlation function has captured some of the qualitative aspects of the low energy excitation scheme exhibited in the RIXS data, a direct comparison between the experiment and the theoretical RIXS spectra may be a next requirement.

As regards the RIXS spectra, no theoretical attempt has been done within the itinerant electron picture. Therefore, in this paper, we formulate the RIXS spectra connected to the density-density correlation function on the basis of the itinerant model introduced in our previous work²⁹. With the revised parameter values of the tight-binding model, we calculate the RIXS spectra within the HFA-RPA scheme. Note that the HFA-RPA scheme has worked well when the antiferromagnetic long-range order is established, even if the system is strongly correlated, such as La_2CuO_4 ^{30,31} and Sr_2IrO_4 ³². In the present case, the HFA to the tight-binding model leads to a magnetic insulator with the zigzag spin order in the ground state, although the energy differences from those of the Néel or stripy orders are obtained as small as ~ 50 meV per Ir ion. We have the energy gap ~ 0.8 eV in the one-electron energy band with the conduction band

composed mainly of the $J_{\text{eff}} = \frac{1}{2}$ states. These results are consistent with the SIC-DFT calculation²⁸.

In formulating the RIXS spectra, we adopt the fast collision approximation (FCA), which is justified when the Ir $2p$ -level life-time broadening width is larger than the relevant excitation energy. Then, the RIXS spectra are connected to the density-density correlation function. We evaluate the formula of the RIXS spectra as a function of ω for momentum transfer \mathbf{q} along symmetry directions within the RPA. We obtain the peaks for $\omega < 20$ meV, which are originated from four bound states in the density-density correlation function below the energy continuum of individual electron-hole pair excitations. The calculated spectra are in qualitative agreement with the RIXS experiments^{10,11}.

The present paper is organized as follows. In Sec. 2, we introduce a multi-orbital tight-binding model and carry out the HFA to the model. In Sec. 3, introducing the dipole transition, we formulate the RIXS spectra in terms of the density-density correlation function within the FCA, which is expressed within the RPA. In Sec. 4, we present the numerical calculations. Section 5 is devoted to the concluding remarks.

II. MODEL AND THE HARTREE-FOCK APPROXIMATION

A. Description of model

Neglecting the crystal distortion, we assume each Ir ion in Na_2IrO_3 resides around the center of oxygen octahedra. The energy level of the e_g orbitals of Ir atom is about 2-3 eV higher than that of the t_{2g} orbitals due to the crystal electric field of IrO_6 . Therefore, taking account of only t_{2g} orbitals, we employ a multi-orbital tight-binding model on a honeycomb lattice, which is defined by

$$H = H_{\text{SO}} + H_{\text{I}} + H_{\text{kin}}, \quad (2.1)$$

with

$$H_{\text{SO}} = \zeta_{\text{SO}} \sum_i \sum_{nn'\sigma\sigma'} d_{in\sigma}^\dagger (\mathbf{L})_{nn'} \cdot (\mathbf{S})_{\sigma\sigma'} d_{in'\sigma'}, \quad (2.2)$$

$$\begin{aligned} H_{\text{I}} = & U \sum_{i,n} n_{in\uparrow} n_{in\downarrow} \\ & + \sum_{i,n < n'\sigma} [U' n_{in\sigma} n_{in'-\sigma} + (U' - J) n_{in\sigma} n_{in'\sigma}] \\ & + J \sum_{i,n \neq n'} (d_{in\uparrow}^\dagger d_{in'\downarrow}^\dagger d_{in\downarrow} d_{in'\uparrow} + d_{in\uparrow}^\dagger d_{in'\downarrow}^\dagger d_{in'\downarrow} d_{in\uparrow}), \end{aligned} \quad (2.3)$$

$$H_{\text{kin}} = \sum_{\langle i,i' \rangle} \sum_{n,n'\sigma} [\hat{T}_{i,i'}]_{n,n'} d_{in\sigma}^\dagger d_{i'n'\sigma} + \text{H.c.}, \quad (2.4)$$

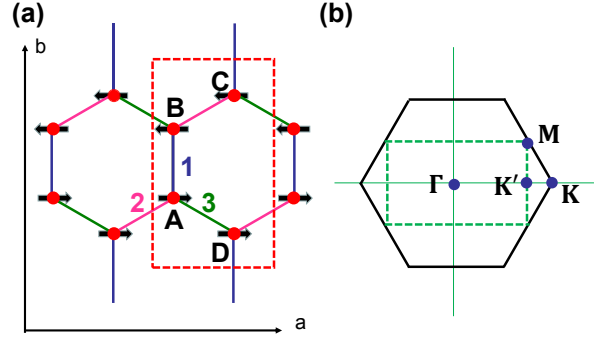


Figure 1: (a) Unit cell for the zigzag ordered phase in a honeycomb lattice. It consists of Ir atoms A, B, C, and D, which is enclosed by a broken line. The attached numbers 1, 2, 3 indicate the types of bonds. Arrows illustrate the zigzag spin ordering pattern. (b) Corresponding magnetic Brillouin zone, which is enclosed by a broken line.

where the annihilation ($d_{in\sigma}$) and creation ($d_{in\sigma}^\dagger$) operators are for the $5d$ electron with orbital n ($= yz, zx, xy$) and spin σ at the Ir site i , and $n_{in\sigma} \equiv d_{in\sigma}^\dagger d_{in\sigma}$.

The H_{SO} stands for the SOI of $5d$ electrons with \mathbf{L} and \mathbf{S} denoting the orbital and spin angular momentum operators, respectively. The H_{I} represents the Coulomb interaction among the t_{2g} electrons, satisfying $U = U' + 2J$ ³³. We use the values $\zeta_{\text{SO}} = 0.45$ eV, $U = 1.4$ eV, and $J/U = 0.15$ in the following calculation. Similar values of the parameters have been utilized for Ir atom in Sr_2IrO_4 ³².

The H_{kin} stands for the kinetic energy of $5d$ electrons with the hopping matrix $\hat{T}_{i,i'}$ between the sites i and i' . The summation $\langle i, i' \rangle$ is restricted within the nearest neighbor Ir ions. There exist two kinds of transfer mechanisms between the Ir $5d$ orbitals. The first one is a direct transfer between the Ir $5d$ orbitals, which may be described by means of the Slater-Koster parameters, $V_{dd\sigma}$, $V_{dd\pi}$ ($= -2V_{dd\sigma}/3$), and $V_{dd\delta}$ ($= V_{dd\sigma}/6$)³⁴. We may evaluate $V_{dd\sigma} = -0.511$ eV by applying Harrison's procedure³⁵. The second one is an indirect transfer via oxygen $2p$ -orbitals. Since the energy required for transferring the electron from oxygen $2p$ levels to Ir $5d$ levels is rather large, the effective transfer between $5d$ orbitals may be estimated by the second-order perturbation. Hence the hopping matrix $\hat{T}_{i,i'}^{(pd)}$ may be expressed in a matrix form with the bases $n = yz, zx, xy$ in order:

$$\hat{T}_{i,i'}^{(pd)} = \begin{pmatrix} 0 & 0 & t_p \\ 0 & 0 & 0 \\ t_p & 0 & 0 \end{pmatrix}, \begin{pmatrix} 0 & 0 & 0 \\ 0 & 0 & -t_p \\ 0 & -t_p & 0 \end{pmatrix}, \begin{pmatrix} 0 & -t_p & 0 \\ -t_p & 0 & 0 \\ 0 & 0 & 0 \end{pmatrix}, \quad (2.5)$$

where $\langle i, i' \rangle$ belongs to bonds 1, 2, and 3, respectively, with the bonds defined in figure 1 (a). The t_p may be as large as ~ 0.25 eV, which value is similar to the one used in the study of Sr_2IrO_4 . The opposite sign had been assigned to t_p in our previous paper²⁹.

B. Hartree-Fock Approximation

We carry out the HFA by following the procedure given in²⁹. In that process, we rewrite the Hamiltonian in terms of the Fourier transformed operator with the wave vector \mathbf{k} within the first magnetic Brillouin zone (MBZ) shown in figure 1(b):

$$d_{\lambda n\sigma}(\mathbf{k}) = (4/N)^{\frac{1}{2}} \sum_{i \in \lambda} d_{in\sigma} e^{-i\mathbf{k} \cdot \mathbf{r}_i}. \quad (2.6)$$

Here, λ specifies one of the four sublattices A, B, C, and D, and N is the number of Ir ions. The first MBZ is divided into 40×40 meshes in the numerical calculation. The parameter values are set $\zeta_{\text{SO}} = 0.45$ eV, $U = 1.4$ eV, $J/U = 0.15$, $V_{dds} = -0.511$ eV, and $t_p = 0.25$ eV.

The staggered magnetic moment is known to be directing to the a axis by the experiment¹⁷. Fixing the staggered moment parallel to the a axis, we carry out the HFA to evaluate the energies of the zigzag, Néel, and stripy ordered states. We find the zigzag ordered state is the most stable. Its energy per Ir ion is 0.09 eV and 0.04 eV smaller than that of the Néel ordered state and that of the stripy ordered state, respectively. The orbital and spin moments align anti-parallel to each other at each site, and their magnitudes are $|\langle L_a \rangle| = 0.51$ and $|\langle S_a \rangle| = 0.16$, respectively, where $\langle X \rangle$ represents the ground state average of operator X . Hence the total magnetic moment is evaluated as $0.19 \mu_B$, which is comparable to the experimental value of $0.22 \mu_B$.

Figure 2 shows the one-electron energy as a function of \mathbf{k} along symmetry directions in the zigzag ordered state. Each line is doubly degenerate. Hence there exist four states per unit cell in the conduction band. The energy gap is found as large as ~ 0.8 eV, and the dependence on \mathbf{k} is rather weak. The " $j_{\text{eff}} = \frac{1}{2}$ " states have the largest weight for the conduction band. The band gap seems overestimated in comparison with the SIC-DFT calculation²⁸.

III. FORMULATION OF RIXS SPECTRA

A. Dipole transition at the Ir L edge

In the dipole transition, the $2p$ core-electron is excited to the $5d$ states by absorbing photon at the L edge (and the reverse process). This process may be described by the interaction

$$H_x = \sum_i \sum_{n,\sigma,j_c,m,\alpha} w(n\sigma; j_c m; \alpha) \times \sum_{\mathbf{q}} [d_{in\sigma}^\dagger p_{ij_c m} c_\alpha(\mathbf{q}) e^{i\mathbf{q} \cdot \mathbf{r}_i} + \text{H.c.}], \quad (3.1)$$

where $c_\alpha(\mathbf{q})$ is the annihilation operator of photon with momentum \mathbf{q} and polarization α . The $p_{ij_c m}$ is the annihilation operator of core electron with the angular momentum j_c ($= \frac{3}{2}, \frac{1}{2}$), and magnetic quantum number m

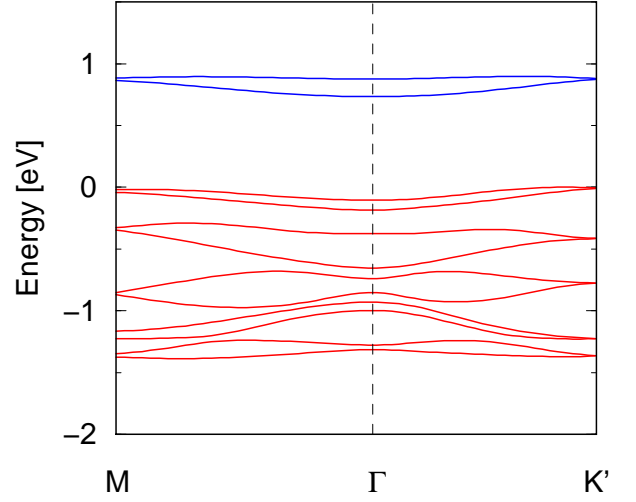


Figure 2: One-electron energy as a function of \mathbf{k} along symmetry directions within the HFA. Parameters are set $V_{dds} = -0.511$ eV, $t_p = 0.25$ eV, $\zeta_{\text{SO}} = 0.45$ eV, $U = 1.4$ eV, and $J/U = 0.15$. The origin of energy is set at the top of the valence band. Each band is doubly degenerate.

at site i . The $w(n\sigma; j_c m; \alpha)$ represents the matrix elements of the $2p \rightarrow 5d$ transition, which explicit values for $\alpha = x, y$, and z are listed in Table I of³². In the Fourier transform representation, (3.1) may be rewritten as

$$H_x = \sum_{\lambda,n,\sigma,j_c,m,\alpha} w(n\sigma; j_c m; \alpha) \times \sum_{\mathbf{k},\mathbf{q}} [d_{\lambda n\sigma}^\dagger ([\mathbf{k} + \mathbf{q}]) p_{\lambda j_c m}(\mathbf{k}) c_\alpha(\mathbf{q}) e^{-i\mathbf{G} \cdot \mathbf{a}_\lambda} + \text{H.c.}], \quad (3.2)$$

with

$$p_{\lambda j_c m}(\mathbf{k}) = (4/N)^{\frac{1}{2}} \sum_i p_{ij_c m} e^{-i\mathbf{k} \cdot \mathbf{r}_i}, \quad (3.3)$$

where \mathbf{k} is defined on the first MBZ in the honeycomb lattice. The photon momentum \mathbf{q} is now regarded as the photon momentum projected onto the two-dimensional ab plane. Here $[\mathbf{k} + \mathbf{q}]$ indicates the vector reduced back to the MBZ by a reciprocal vector \mathbf{G} , that is, $\mathbf{k} + \mathbf{q} = [\mathbf{k} + \mathbf{q}] + \mathbf{G}$, and \mathbf{a}_λ is defined by $(0,0)$, $(0,1)$, $(\sqrt{3}/2, 3/2)$, and $(\sqrt{3}/2, -1/2)$ in units of a (the nearest neighbor distance) for $\lambda = A, B, C$, and D , respectively.

B. Second-order optical process and the scattering geometry

The RIXS spectral intensity may be expressed by the second-order optical process,

$$W(\omega_i, q; \alpha_i, \alpha_f) = 2\pi \sum_{f'} \left| \sum_n \frac{\langle \Phi_{f'} | H_x | \Phi_n \rangle \langle \Phi_n | H_x | \Phi_i \rangle}{\omega_i + \epsilon_g - \epsilon_n + i\Gamma_c} \right|^2 \times \delta(\omega_i + \epsilon_g - \omega_f - \epsilon_{f'}), \quad (3.4)$$

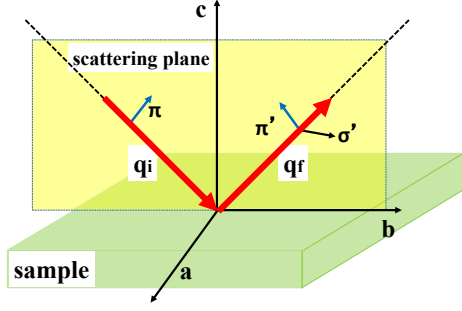


Figure 3: Horizontal scattering geometry. The scattering plane is assumed to be perpendicular to the ab plane, and is including the b axis.

where the initial state $|\Phi_i\rangle$ may be expressed by $c_{\alpha_i}^\dagger(\mathbf{q}_i)|0\rangle|g\rangle$ with $|g\rangle$ denoting the ground state of the matter with energy ϵ_g , and $|0\rangle$ denoting the vacuum state with photon, respectively. The intermediate state $|\Phi_n\rangle$ may be expressed by $|0\rangle|n\rangle$ with $|n\rangle$ denoting the intermediate state of the matter with energy ϵ_n , and Γ_c stands for the life-time broadening width of the $2p$ -core hole state. The state $|\Phi_{f'}\rangle$ may be expressed by $c_{\alpha_f}^\dagger(\mathbf{q}_f)|0\rangle|f'\rangle$ with $|f'\rangle$ denoting the excited state of the matter with energy $\epsilon_{f'}$. The incident photon has momentum and energy $q_i = (\mathbf{q}_i, \omega_i)$ with polarization α_i , while the scattered photon has momentum and energy $q_f = (\mathbf{q}_f, \omega_f)$ with polarization α_f . The momentum and energy transferred to the matter are accordingly given by $q = q_i - q_f = (\mathbf{q}, \omega)$.

Most of RIXS experiments have been carried out in a horizontal scattering geometry with the scattering angle 2θ set to be close to 90° . In the following analysis, we tentatively assume that the scattering plane is perpendicular to the plane of honeycomb, and is including the b axis, as illustrated in figure 3. Note that only a few degrees of tilt of the scattering plane could sweep the entire Brillouin zone, since $\omega \sim 11.2$ keV at the Ir L_3 edge. In the coordinate frame with a , b , and c axes, the polarization vectors are given by

$$\alpha_i = \left(0, \frac{1}{\sqrt{2}}, \frac{1}{\sqrt{2}}\right), \text{ for } \pi \text{ polarization}, \quad (3.5)$$

$$\alpha_f = \begin{cases} (1, 0, 0), & \text{for } \sigma' \text{ polarization,} \\ \left(0, -\frac{1}{\sqrt{2}}, \frac{1}{\sqrt{2}}\right), & \text{for } \pi' \text{ polarization.} \end{cases} \quad (3.6)$$

Note that the t_{2g} states, yz , zx , and xy , as well as the polarizations in $w(n\sigma; j_c m; \alpha)$ are defined in the cubic coordinate frame.

C. Fast collision approximation

Since the value of Γ_c (~ 2.5 eV) is much larger than a variation of ϵ_n with n , the energy denominator of (3.4) could be factored out in a reasonable accuracy. This procedure is called as the FCA, and (3.4) may be rewritten

as

$$W(\omega_i, q; \alpha_i, \alpha_f) = 2\pi |R(\omega_i, E_0)|^2 \sum_{f'} \left| \sum_n \langle \Phi_{f'} | H_x | \Phi_n \rangle \langle \Phi_n | H_x | \Phi_i \rangle \right|^2 \delta(\omega + \epsilon_g - \epsilon_{f'}) \quad (3.7)$$

with

$$R(\omega_i, E_0) = \frac{1}{\omega_i - E_0 + \epsilon_{2p}(j_c) + i\Gamma_c}, \quad (3.8)$$

where E_0 stands for a typical energy of the conduction band. Using the Fourier transform representation, (3.7) is rewritten as,

$$W(\omega_i, q; \alpha_i, \alpha_f) = |R(\omega_i, E_0)|^2 \hat{M}^\dagger(\alpha_i, \alpha_f; j_c) \hat{Y}^{+-}(q) \hat{M}(\alpha_i, \alpha_f; j_c), \quad (3.9)$$

where

$$\begin{aligned} [\hat{M}(\alpha_i, \alpha_f; j_c)]_{\xi\xi'} &= \delta_{\lambda, \lambda'} \sum_m \sum_{\alpha, \alpha'} (\alpha_i)_\alpha w(n\sigma; j_c m; \alpha) \\ &\times w^*(n'\sigma'; j_c m; \alpha') (\alpha_f)_{\alpha'}, \end{aligned} \quad (3.10)$$

with $\xi = (\lambda, n, \sigma)$ and $\xi' = (\lambda', n', \sigma')$. The summations for α and α' run over x, y , and z . The $\hat{M}(\alpha_i, \alpha_f; j_c)$ is regarded as a vector with 576 dimensions. The $\hat{Y}^{+-}(q)$ represents the generalized density-density correlation function defined by

$$[\hat{Y}^{+-}(\mathbf{q}, \omega)]_{\xi_1 \xi'_1; \xi \xi'} = \int_{-\infty}^{\infty} \langle [\rho_{\mathbf{q}\xi_1 \xi'_1}(t)]^\dagger \rho_{\mathbf{q}\xi \xi'}(0) \rangle e^{i\omega t} dt, \quad (3.11)$$

with

$$\rho_{\mathbf{q}\xi \xi'} = (4/N)^{\frac{1}{2}} \sum_{\mathbf{k}} d_\xi^\dagger([\mathbf{k} + \mathbf{q}]) d_{\xi'}(\mathbf{k}) e^{-i\mathbf{G} \cdot \mathbf{a}_\lambda}. \quad (3.12)$$

Thereby $\hat{Y}^{+-}(q)$ is a matrix of 576×576 dimensions. Since an extra phase factor $e^{-i\mathbf{G} \cdot \mathbf{a}_\lambda}$ is contained in (3.12), the RIXS intensities may become different between the inside and the outside of the first MBZ.

D. $\hat{Y}^{+-}(q)$ within the RPA

Now that the RIXS spectra are connected with the density-density correlation function, we outline the procedure to calculate it within the RPA. See²⁹ for details.

Let us introduce the two-particle Green's function,

$$[\hat{Y}^T(q)]_{\xi_1 \xi'_1; \xi \xi'} = -i \int \langle T \{ [\rho_{\mathbf{q}\xi_1 \xi'_1}(t)]^\dagger \rho_{\mathbf{q}\xi \xi'}(0) \} \rangle e^{i\omega t} dt, \quad (3.13)$$

where T denoting the time ordering operator and $X(t) \equiv e^{iHt} X e^{-iHt}$. By taking account of the multiple scattering between particle-hole pair, it is expressed as

$$\hat{Y}^T(q) = \hat{F}(q) [\hat{I} + \hat{F}(q)]^{-1} = [\hat{F}(q)^{-1} + \hat{I}]^{-1}, \quad (3.14)$$

where $\hat{\Gamma}$ stands for the antisymmetrized vertex function, which is expressed as

$$[\hat{\Gamma}]_{\xi_2\xi'_2;\xi_1\xi'_1} = g(\xi_2\xi'_1;\xi_1\xi'_2) - g(\xi_2\xi'_1;\xi'_2\xi_1), \quad (3.15)$$

with g defined by the coefficient in the Coulomb interaction,

$$H_I = \frac{1}{2} \sum_i \sum_{\nu_1, \nu_2, \nu_3, \nu_4} g(\nu_1\nu_2; \nu_3\nu_4) d_{i\nu_1}^\dagger d_{i\nu_2}^\dagger d_{i\nu_4} d_{i\nu_3}. \quad (3.16)$$

Then, $\hat{F}(q)$ in (3.14) is defined as

$$[\hat{F}(q)]_{\xi_2\xi'_2;\xi_1\xi'_1} \equiv -i \frac{4}{N} \sum_{\mathbf{k}} \int \frac{dk_0}{2\pi} [\hat{G}(\mathbf{k} + \mathbf{q}, k_0 + \omega)]_{\xi_2\xi_1} \times [\hat{G}(\mathbf{k}, k_0)]_{\xi'_1\xi'_2} e^{i\mathbf{G} \cdot (\mathbf{a}_{\lambda_2} - \mathbf{a}_{\lambda_1})}, \quad (3.17)$$

where $\hat{G}(\mathbf{k}, \omega)$ stands for the single-particle Green's function:

$$[\hat{G}(\mathbf{k}, \omega)]_{\xi, \xi'} = -i \int \langle T[d_\xi(\mathbf{k}, t) d_{\xi'}^\dagger(\mathbf{k}, 0)] \rangle e^{i\omega t} dt. \quad (3.18)$$

This may be written within the HFA as

$$[\hat{G}(\mathbf{k}, \omega)]_{\xi, \xi'} = \sum_{\ell} \frac{[\hat{U}(\mathbf{k})]_{\xi, \ell} [\hat{U}(\mathbf{k})^{-1}]_{\ell, \xi'}}{\omega - E_\ell(\mathbf{k}) + i\delta \text{sgn}[E_\ell(\mathbf{k})]}, \quad (3.19)$$

where $\text{sgn}[A]$ stands for a sign of quantity A and δ denotes a positive convergent factor. The $E_\ell(\mathbf{k})$ and $[\hat{U}(\mathbf{k})]_{\xi, \ell}$ stand for the ℓ -th energy eigenvalue measured from the chemical potential and the corresponding wave function, respectively. By inserting (3.19) into (3.17), we have

$$\begin{aligned} [\hat{F}(q)]_{\xi_2\xi'_2;\xi_1\xi'_1} &= \frac{4}{N} \sum_{\mathbf{k}} \sum_{\ell, \ell'} U_{\xi_2\ell}(\mathbf{k} + \mathbf{q}) U_{\xi_1\ell}^*(\mathbf{k} + \mathbf{q}) \\ &\times U_{\xi'_1\ell'}(\mathbf{k}) U_{\xi'_2\ell'}^*(\mathbf{k}) e^{i\mathbf{G} \cdot (\mathbf{a}_{\lambda_2} - \mathbf{a}_{\lambda_1})} \\ &\times \left[\frac{[1 - n_\ell(\mathbf{k} + \mathbf{q})] n_{\ell'}(\mathbf{k})}{\omega - E_\ell(\mathbf{k} + \mathbf{q}) + E_{\ell'}(\mathbf{k}) + i\delta} \right. \\ &\quad \left. - \frac{n_\ell(\mathbf{k} + \mathbf{q}) [1 - n_{\ell'}(\mathbf{k})]}{\omega - E_\ell(\mathbf{k} + \mathbf{q}) + E_{\ell'}(\mathbf{k}) - i\delta} \right]. \end{aligned} \quad (3.20)$$

Once we obtain the two-particle Green's function $\hat{Y}^T(q)$, we can evaluate the density-density correlation function $\hat{Y}^{+-}(q)$ with the help of the fluctuation-dissipation theorem,

$$[\hat{Y}^{+-}(q)]_{\xi_1\xi'_1;\xi\xi'} = i \left\{ [\hat{Y}^T(q)]_{\xi_1\xi'_1;\xi\xi'} - [\hat{Y}^T(q)]_{\xi\xi';\xi_1\xi'_1}^* \right\}. \quad (3.21)$$

IV. CALCULATED RESULTS

In addition to the continuous states of individual electron-hole pair excitations, there emerge several

bound states as poles in $\hat{Y}^{+-}(q)$. To obtain such bound states, we search for ω giving zero eigenvalue in $\hat{F}(q)^{-1} + \hat{\Gamma}$. In this procedure, we evaluate $\hat{F}(q)$ by summing over \mathbf{k} in (3.20) with dividing the MBZ into 40×40 meshes. Let $\omega_B(\mathbf{q})$ be the bound-state energy. Then the residue of the pole, which is necessary to calculate the spectral intensity, is evaluated by finite difference between $\omega = \omega_B(\mathbf{q})$ and $\omega = \omega_B(\mathbf{q}) + 0.0001\text{eV}$ in place of the differentiation. In order to compare the calculated RIXS spectra with those of the experiment, we should specify the polarization setting. As given in (3.5) and (3.6), the incident photon with π -polarization is prepared, then, the scattered photons have been collected without separating the σ' and π' polarizations in the experiment¹¹. Thus, all the results shown in this section represent the sum of the spectra in the $\pi - \sigma'$ and $\pi - \pi'$ channels.

A. Magnetic excitations

Panel (a) in figure 4 shows the calculated bound-state energy $\omega_B(\mathbf{q})$ as a function of \mathbf{q} along the symmetry directions in the low-energy region. We find that four gapped excitation modes reside below 20 meV, which may be identified as magnetic excitations. Such small energy scale is consistent with the energy difference between the zigzag and other magnetic orders discussed in Sec. II B. The presence of four modes may be consistent with the spin-wave excitations in the localized $j_{\text{eff}} = \frac{1}{2}$ spin model in the zigzag ordered state. At the K' point, four modes become two pairs of degenerate modes. Experimentally, the magnetic excitations have been identified below 6 meV by INS¹² and found extending up to 35 meV by RIXS¹¹. It suggests there exist at least two magnetic excitation modes, which is consistent with our results. Finally, the excitation energy becomes smaller with \mathbf{q} away from the Γ point in qualitative agreement with the RIXS experiment¹¹.

Panels (b) and (c) in figure 4 show the RIXS spectra as a function of ω for \mathbf{q} from the Γ to the M points and the Γ to K' points, respectively. The δ -function peaks are convoluted with the Lorentzian function with the half width of half maximum 1 meV. Among four modes, two upper-energy modes have intensities much larger than two lower-energy modes in the present scattering geometry.

B. Excitonic excitations

Following the same procedure as the magnetic excitations, we find sixteen bound states for $0.4 < \omega_B(\mathbf{q}) < 0.8$ eV below the energy continuum of individual electron-hole pair excitations in the density-density correlation function, which may be identified as excitonic excitations. They are composed mainly of a pair of $j_{\text{eff}} = \frac{1}{2}$ electron and $j_{\text{eff}} = \frac{3}{2}$ hole. The presence of sixteen modes may

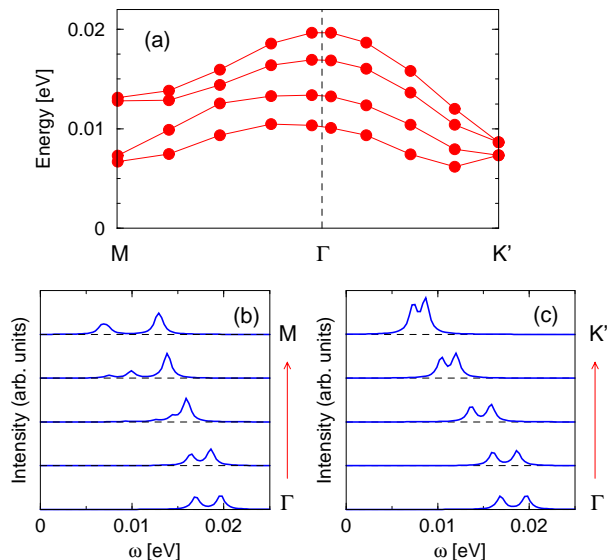


Figure 4: Panel (a): Dispersion relation of magnetic excitations for \mathbf{q} along symmetry directions. Panels (b) and (c): RIXS spectra in a horizontal scattering geometry as a function of ω for \mathbf{q} from the Γ to the M points, and from the Γ to the K' points. Intensities of the σ and π polarizations are summed for the scattered x-ray. The spectra are convoluted with the Lorentzian function with half width of half maximum 1 meV.

be consistent with the localized excitations from $j_{\text{eff}} = \frac{3}{2}$ to $\frac{1}{2}$ states for four Ir ions in the unit cell of the zigzag ordering state. The continuous spectra are roughly estimated by sorting $E_{\ell}(\mathbf{k} + \mathbf{q}) - E_{\ell'}(\mathbf{k})$ into segments with the width 0.05 eV in (3.20), resulting in a histogram representation.

Figure 5 shows the calculated RIXS spectra as a function of ω for \mathbf{q} from the Γ to the K' points. The spectra are convoluted with the Lorentzian function with the half width of half maximum 0.04 eV. Arrows indicate the lowest boundary of the energy continuum. We have three prominent peaks. In the RIXS experiment, three peaks named A, B, and C have been observed at $\omega \sim 0.42$ eV, 0.72 eV, and 0.83 eV, respectively, with little momentum dependence¹⁰. The structure found in our calculated spectra seems to agree qualitatively with that derived from the calculation on a small cluster³⁶ and the experimental spectra¹⁰.

V. CONCLUDING REMARKS

We have analyzed RIXS spectra in Na_2IrO_3 on a multi-orbital tight-binding model composed only of the t_{2g} orbitals for Ir ions on a honeycomb lattice. Using conventional parameter values for the SOI, the Coulomb interaction, and the Ir-Ir transfer energy, we have carried out the HFA to the model to calculate the one-electron energy as well as the ground-state energy by fixing the staggered

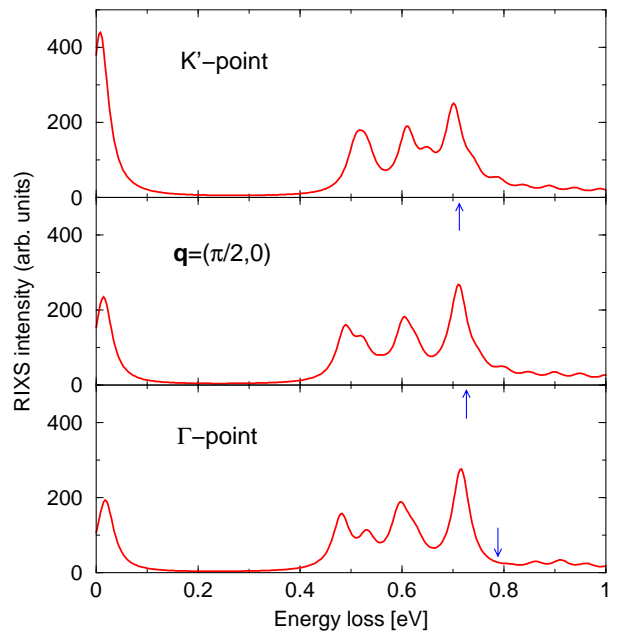


Figure 5: The RIXS spectra for both the magnon and the exciton excitations as a function of ω for \mathbf{q} from the Γ to the K' points. Arrows indicate the lowest boundary of individual electron-hole pair excitations. The spectra are convoluted with Lorentzian function with the half width half maximum 0.04 eV.

magnetic moment along the a axis. The zigzag ordering phase is found stabler than the Néel and the stripy ordering phases. It may be remarkable that the HFA to the simple tight-binding model leads to the zigzag order, since the energy difference from other orders are rather small.

We have formulated the RIXS spectra in terms of the density-density correlation function within the FCA. The RIXS spectra have been evaluated within the RPA. In the correlation function, there appear four bound states below 20 meV, and sixteen bound states between 0.4 and 0.8 eV, below the energy continuum of the individual electron-hole pair excitations. These bound states constitute the spectral peaks, which are in qualitative agreement with the RIXS experiment^{10,11}. Note that the HFA-RPA scheme has worked well for describing the excitation spectra in the presence of the antiferromagnetic long-range order in La_2CuO_4 ^{30,31} and Sr_2IrO_4 ³². The present results are of qualitative nature, based on a simple model and neglecting electron correlations. To be quantitative along the itinerant-electron approach, it may be necessary to use more realistic models, and to go beyond the HFA-RPA.

Acknowledgments

We thank M. Takahashi for valuable discussions. This work was partially supported by a Grant-in-Aid for Sci-

entific Research from the Ministry of Education, Culture, Sports, Science and Technology of the Japanese Govern-

ment.

- ¹ L. J. P. Ament, M. van Veenendaal, T. P. Devereaux, J. P. Hill, and J. van den Brink, *Rev. Mod. Phys.* **83**, 705 (2011).
- ² M. P. M. Dean, *J. Magn. Magn. Mater.* **376**, 3 (2015).
- ³ S. Fatale, S. Moser, and M. Grioni, *J. Electron Spectrosc. Relat. Phenom.* **200**, 274 (2015).
- ⁴ T. Tohyama, *J. Electron Spectrosc. Relat. Phenom.* **200**, 209 (2015).
- ⁵ L. Braicovich, L. J. P. Ament, V. Bisogni, F. Forte, C. Aruta, G. Balestrino, N. B. Brookes, G. M. De Luca, P. G. Medaglia, F. M. Granozio, et al., *Phys. Rev. Lett.* **102**, 167401 (2009).
- ⁶ L. Braicovich, J. van den Brink, V. Bisogni, M. M. Sala, L. J. P. Ament, N. B. Brookes, G. M. De Luca, M. Salluzzo, T. Schmitt, V. N. Strocov, et al., *Phys. Rev. Lett.* **104**, 077002 (2010).
- ⁷ M. Guarise, B. D. Piazza, M. M. Sala, G. Ghiringhelli, L. Braicovich, H. Berger, J. N. Hancock, D. van der Marel, T. Schmitt, V. N. Strocov, et al., *Phys. Rev. Lett.* **105**, 157006 (2010).
- ⁸ M. M. Sala, K. Ohgushi, A. Al-Zein, Y. Hirata, G. Monaco, and M. Krisch, *Phys. Rev. Lett.* **112**, 176402 (2014).
- ⁹ J. Kim, D. Casa, M. H. Upton, T. Gog, Y.-J. Kim, J. F. Mitchell, M. van Veenendaal, M. Daghofer, J. van den Brink, G. Khaliullin, et al., *Phys. Rev. Lett.* **108**, 177003 (2012).
- ¹⁰ H. Gretarsson, J. P. Clancy, X. Liu, J. P. Hill, E. Bozin, Y. Singh, S. Manni, P. Gegenwart, J. Kim, A. H. Said, et al., *Phys. Rev. Lett.* **110**, 076402 (2013).
- ¹¹ H. Gretarsson, J. P. Clancy, Y. Singh, P. Gegenwart, J. P. Hill, J. Kim, M. H. Upton, A. H. Said, D. Casa, T. Gog, et al., *Phys. Rev. B* **87**, 220407(R) (2013).
- ¹² S. K. Choi, R. Coldea, A. N. Kolmogorov, T. Lancaster, I. I. Mazin, S. J. Blundell, P. G. Radaelli, Y. Singh, P. Gegenwart, K. R. Choi, et al., *Phys. Rev. Lett.* **108**, 127204 (2012).
- ¹³ F. Ye, S. Chi, H. Cao, B. C. Chakoumakos, J. A. Fernandez-Baca, R. Custelcean, T. F. Qi, O. B. Korneta, and G. Cao, *Phys. Rev. B* **85**, 180403(R) (2012).
- ¹⁴ S. W. Lovesey and A. N. Dobrynin, *J. Phys.: Condens. Matter* **24**, 382201 (2012).
- ¹⁵ Y. Singh and P. Gegenwart, *Phys. Rev. B* **82**, 064412 (2010).
- ¹⁶ R. Comin, G. Levy, B. Ludbrook, Z.-H. Zhu, C. N. Veenstra, J. A. Rosen, Y. Singh, P. Gegenwart, D. Stricker, J. N. Hancock, et al., *Phys. Rev. Lett.* **109**, 266406 (2012).
- ¹⁷ X. Liu, T. Berlijn, W.-G. Yin, W. Ku, A. Tsvelik, Y.-J. Kim, H. Gretarsson, Y. Singh, P. Gegenwart, and J. P. Hill, *Phys. Rev. B* **83**, 220403(R) (2011).
- ¹⁸ A. Kitaev, *Ann. Phys. (Amsterdam)* **321**, 2 (2006).
- ¹⁹ J. Chaloupka, G. Jackeli, and G. Khaliullin, *Phys. Rev. Lett.* **105**, 027204 (2010).
- ²⁰ I. Kimchi and Y.-Z. You, *Phys. Rev. B* **84**, 180407(R) (2011).
- ²¹ J. Chaloupka, G. Jackeli, and G. Khaliullin, *Phys. Rev. Lett.* **110**, 097204 (2013).
- ²² Y. Sizyuk, C. Price, P. Wölfle, and N. B. Perkins, *Phys. Rev. B* **90**, 155126 (2014).
- ²³ V. M. Katukuri, S. Nishimoto, V. Yushankhai, A. Stoyanova, H. Kandpal, S. Choi, R. Coldea, I. Rousochatzakis, L. Hozoi, and J. van den Brink, *New J. Phys.* **16**, 013056 (2014).
- ²⁴ J. G. Rau, E.-H. Lee, and H.-Y. Kee, *Phys. Rev. Lett.* **112**, 077204 (2014).
- ²⁵ Y. Yamaji, Y. Nomura, M. Kurita, R. Arita, and M. Imada, *Phys. Rev. Lett.* **113**, 107201 (2014).
- ²⁶ I. I. Mazin, H. O. Jeschke, K. Foyevtsova, R. Valentí, and D. I. Khomskii, *Phys. Rev. Lett.* **109**, 197201 (2012).
- ²⁷ K. Foyevtsova, H. O. Jeschke, I. I. Mazin, D. I. Khomskii, and R. Valentí, *Phys. Rev. B* **88**, 035107 (2013).
- ²⁸ H.-J. Kim, J.-H. Lee, and J.-H. Cho, *Sci. Rep.* **4**, 5253 (2014).
- ²⁹ J. Igarashi and T. Nagao, *J. Phys.: Condens. Matter* **28**, 026006 (2016).
- ³⁰ T. Nomura and J. I. Igarashi, *Phys. Rev. B* **71**, 035110 (2005).
- ³¹ T. Nomura, *J. Phys. Soc. Jpn.* **84**, 094704 (2015).
- ³² J. Igarashi and T. Nagao, *Phys. Rev. B* **90**, 064402 (2014).
- ³³ J. Kanamori, *Prog. Theor. Phys.* **30**, 275 (1963).
- ³⁴ J. C. Slater and G. F. Koster, *Phys. Rev.* **94**, 1498 (1954).
- ³⁵ W. A. Harrison, *Elementary Electronic Structure* (Singapore:World Scientific, 2004).
- ³⁶ B. H. Kim, G. Khaliullin, and B. I. Min, *Phys. Rev. B* **89**, 081109(R) (2014).